The International Journal of Advanced Manufacturing Technology (2023) 129:3849–3861
https://doi.org/10.1007/s00170-023-12522-7

ORIGINAL ARTICLE

Thermomechanical effect on the properties of stainless steels using rotative friction welding: an experimental study on 304L and 316L grades

Fatima Zohra Arzour[1] · Mouna Amara[1] · Rami K. Suleiman[2] · Mohammed Hadj Meliani[1,3]

Received: 18 August 2023 / Accepted: 13 October 2023 / Published online: 1 November 2023

Abstract
The main objective of this work is to analyze structural hardening by direct friction welding on two austenitic materials of the AISI 304L and AISI 316L series that were welded separately (similar welding) followed by a combined (mixed) welding. The friction welding parameters such as rotation speed, applied pressure (friction and forging), and holding time were carefully selected and optimized. Forty welding operations and thirty post-welding nominal tensile tests were performed, with the sole purpose of obtaining the rational curves. To achieve this objective, the results of the tensile tests were collected and analyzed. The rational curves allowed us to proceed by classical analytical modeling to quantify the effect of welding on the work-hardening behavior of the two stainless steel samples. The microstructure of each welded joint condition was analyzed and compared to each other.

Keywords Friction · Welding · Optimization · Analytical model · Weld joint

1 Introduction

Austenitic steels, and more precisely, AISI 304L and AISI 316L, are becoming indispensable in many fields, such as nuclear, building and public works, shipbuilding, automotive, aeronautics, tooling, mechanical industry, food industry, chemicals, transportation, and medical [1]. This wide scope of use of these ready materials in various industrial applications can be extended to welding applications due to their impressive characteristics such as elastic limit, ductility, resistance to corrosion and oxidation, weldability, formability, and level of toughness.

In the current study, we are interested in direct friction welding as a solid-state bonding process, in which this process can utilize the heat generated between two friction surfaces [2]. This process uses two phases: (i) friction and (ii) forging [3]. Major parameters can control the processes which are the rotational speed, force, and holding time of the friction phase and the forging phase [4]. The microstructure produced in the welded joint can be strongly affected by the strain hardening of the mechanical properties of the base materials. This process is of great interest to contemporary researchers, in particular, in the case of using austenitic steels [5–7]. The previously published studies in this field have generally focused on the effect and optimization of the abovementioned parameters for obtaining joint properties that are as close as possible to the base material.

During the last two decades, extensive works have been conducted and reported on the austenitic steels in particular. Ozdemir [8], for example, has comprehensively analyzed the effect of the variation of the rotation speed during a direct friction welding operation, carried out on bars of 12 mm in diameter using two austenitic steels, AISI 304L and AISI

✉ Mohammed Hadj Meliani
m.hadjmeliani@univ-chlef.dz

Fatima Zohra Arzour
fz.arzour@univ-chlef.dz

Mouna Amara
m.amara@univ-chlef.dz

Rami K. Suleiman
ramismob@kfupm.edu.sa

[1] Laboratory for Theoretical Physics and Material Physics (LPTPM), Hassiba Benbouali University of Chlef, P.O. Box. 151, 02000 Hay Salem, Algeria

[2] Interdisciplinary Research Center for Advanced Materials, King Fahd University of Petroleum & Minerals (KFUPM), Dhahran 31261, Saudi Arabia

[3] L3EM, Lorraine University, 57070 Metz, France

4340. The study found that a rotation speed of about 2500 rpm increased the tensile strength of the post-weld joint. In another study [8] conducted on aluminum alloy AA6082 and austenitic stainless steel AISI 304, the authors showed that the friction force has a great impact on the tensile strength of the produced joint with an order of two times compared to maintaining the friction and forging. In the same direction, Ananda et al. [9] performed mixed welding operations on bar samples (20 mm in diameter) taken from AISI 1010 and ASTM B22 standards. The authors found that the optimal process was for a friction force of 20 MPa, a forging force of 22 MPa, and a forging time of 5 s. Another friction welding experiment on two other steels AISI 316L and 1045 MCS showed that the increase in the forging force of the interface hardness can induce an increase and the ultimate tensile strength and a decrease in the ductility. Other authors [10] have observed that a failure at the joint turn has occurred on the heat affected zone (HAZ) side of AISI 316L. As a result of this, the study found that the forging force has a positive effect on the evolution of mechanical properties around the interface of the welded joint.

Through this work, our interest was to analyze the effect of strain hardening that is generated by direct friction welding (RFW) on two materials of the AISI series, namely 304 and 316. We gave also make attention to the evolution of the flow stress and the post-welding ductility. To this end, the previously published works by Ludwik's law [11], Hollomon's law [12], Swift's law [13], and finally Ludwigson's law [14] were conducted on forty welding operations and thirty standardized post-welding tensile tests with the main objective of identifying the parameters of work hardening, using four well-known laws of behavior.

After that, an analysis via these four analytical laws was conducted using several combinations of welding operations, on joints obtained by the use of similar and combined (mixed) materials, aiming to quantify the level of degradation of certain mechanical properties and, in particular, the flow stress and ductility with the evolution of the temperature. To the best of our knowledge, few works have been reported in the literature on the hardening behavior and its evolution after direct friction welding. In this trajectory, Kumar et al. [15] have used four temperatures (ambient, 550, 600, and 650 °C) to account for the degradation in the mechanical properties of Super 304HCu steel upon reducing the temperature. Using Hollomon's law, the obtained prediction results showed that the strain hardening occurred in two stages. Similarly, Kashyap et al. [16, 17] have tested a range of temperature values from 21 to 900 °C on the tensile performance of the AISI 316L substrate. They found that the rate of deformation varied from 10^{-5} to 10^{-3} s^{-1} and the presence of two to three distinct rates of deformation. Similarly, Li et al. [18, 19] have arrived at the same conclusion based on the results of tensile tests performed on AISI 316L and AISI 316LN substrates cold-rolled previously. Using two behavior laws, Hollomon's and Ludwigson's, they concluded that the post-processing behavior can be correctly described by Ludwigson's law, which was further confirmed by the results of the tensile tests on cold-rolled samples of the aforementioned substrates.

2 Experimental tests and process parameters

Friction welding (RFW) between two surfaces generates a heat flow around the interface, where the first sample is fixed and rotated, and the second moves linearly under the effect of an axial force. The movement of the two parts on either side causes the temperature to rise to 1000 °C under certain conditions related to the two surfaces in friction and the conductivity of the used material and its diameter. This temperature level brings the solid material around the interface to a pasty state. Naturally, as the friction decreases, the temperature starts to drop in the open air due to the effect of the rotation. From our reported work in Ref. [20], the process involved stopping the rotation, announcing the beginning of the forging phase, creating immediately a new zone of deformation by contact, accentuating the consumption of the material, and giving the final shape of the bead (Fig. 1).

The tensile tests were performed on a universal testing machine INSTRON 5500 with a load capacity of ± 100 kN. All tests were performed under the same welding conditions and under a quasi-static strain rate of 1.6×10^{-3} s^{-1}. Whatever the joint configuration of the specimens, they were of 45 mm in length and 12 mm in diameter and were cut in the axial direction according to the standard specification of ISO 6892-1: 2009 (F); directly from bars of 6 m, the line of the joint interface was placed in the center of the specimen. This

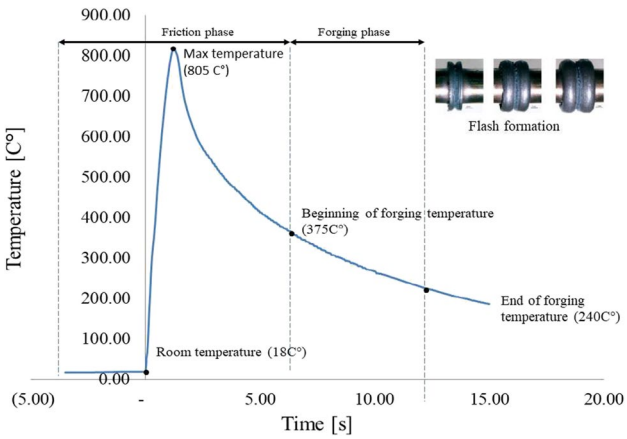

Fig. 1 Different zones of deformations after increasing the temperature contact as a function of time [20]

allowed the use of an extensometer and putting it on either side of the joint interface.

To describe the effect of time of the friction phase on the behavior of the welded joint, we have used four laws of behavior as follows:

Ludwik's law:

$$\sigma = \sigma + K - -_L \varepsilon_P{}^{n_L} \tag{1}$$

$$\ln\left(\sigma - \sigma_0\right) = \ln\left(K_L\right) + n_L \ln\left(\varepsilon_p\right) \tag{2}$$

Hollomon's law:

$$\sigma = K_H \varepsilon_P{}^{n_H} \tag{3}$$

$$\ln\left(\sigma\right) = \ln\left(K_s\right) + n_s \ln\left(\varepsilon_0 + \varepsilon_P\right) \tag{4}$$

Swift's law:

$$\sigma = K_s\left(\varepsilon_0 + \varepsilon_P\right)^{n_s} \tag{5}$$

$$\ln\left(\sigma\right) = \ln\left(K_H\right) + n_H \ln\left(\varepsilon_P\right) \tag{6}$$

Ludwigson's law:

$$\sigma = \mathrm{K}_1 \varepsilon_1{}^{n_1} + \exp\left(K_2 + n_2 \varepsilon_P\right) \tag{7}$$

$$\sigma_1 = K_1 \varepsilon_1{}^{n_1} \tag{8}$$

$$\Delta = \exp\left(K_2 + n_2 \varepsilon_P\right) \tag{9}$$

where rational stress, σ_0: threshold stress, K: strain hardening coefficient, ε_0: threshold deformation, ε_p: plastic deformation, n_L, n_H, and n_S: Ludwik's, Hollomon's, and Swift's squaring coefficients, respectively; K_1, n_1: coefficients of strength and strain hardening of Hollomon, K_2, n_2: Ludwigson's strength and strain hardening coefficients.

The work of Ludwigson [10] considered the Holloman [11] relationship not capable of describing the plastic behavior at low strains for the stable stainless steel and face-centered cubic metals with low stacking-fault energy (SFE). They have proposed the modified equation listed as Eq. (7) to account for the significant positive deviations at low strain. The second term on the right-hand side that dominates at low strain indicates planar slip while the first term that dominates at high strain represents cross-slip and cell formation. Furthermore, Samuel [21] extended the modified Ludwigson formulation to all materials, regardless of SFE. He pointed out that the deviation at low strains is a consequence of some unknown "plastic strain equivalent" presented in materials. The second term was added to the Ludwik model to account for the deviations at low strains for stable austenitic stainless steels and other face-centered cubic (fcc) metals with low stacking fault energies. The applicability of the Ludwik equations found that the uniform strain values depend on the equation used. The calculated uniform strain values were found to depend on the equation used. Even when the Hollomon equation gave a high linear correlation coefficient in log-log coordinates, the strain hardening exponent "n" could give an erroneous uniform strain. The equation with the lowest standard error of estimate gave the uniform strain nearest to the value obtained by direct measurement from the load-elongation curve [14].

3 Results

3.1 Nominal tensile tests

The nominal tensile curves were recorded in stress-strain, concerning the base metal and the welded joints, using AISI 316 and AISI 304 (Fig. 2). The post-weld mechanical properties of these two metals are summarized in Table 1. Each test was repeated several times to maintain the validity of the obtained results, especially for the control of symmetry of the specimens, the application of the centered load, and the final process. The range of test pieces of samples was between 5 and 11 (Fig. 3).

3.2 Identification of the hardening laws' parameters

The first law used to describe the mechanical behavior of metals during strain hardening is Ludwik's law, used since the year 1909 and expressed by Eq. 1, with σ_0, the threshold stress, determined from a tensile test, symbolized by K_L and n_L obtained by linear regression plotting of the curve in Eq. 2, shown in Fig. 4. The use

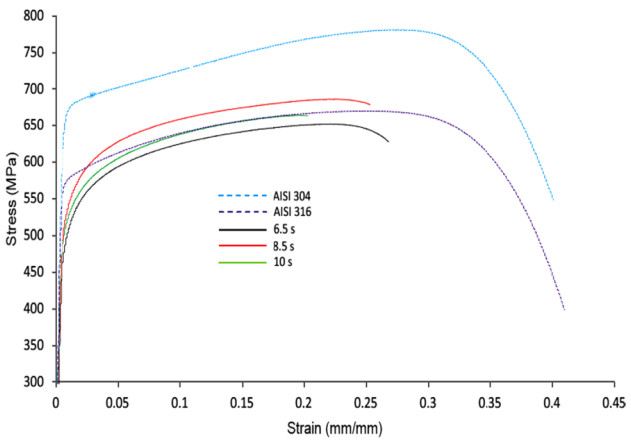

Fig. 2 An example of the nominal tension curve of friction welding operation

Table 1 Post-weld mechanical properties of the two AISI 304L metals

	σ_0 (MPa)	ε_0	σ_{max} (MPa)	ε_{max}
Base metal AISI 304L	618.74	0.005	781.41	0.468
Base metal AISI 316L	541.47	0.005	678.19	0.457
Welded joint AISI 304L				
pdf. = 0 MPa	499.59	0.004	718.11	0.327
pdf. = 280 MPa	502.91	0.004	703.68	0.324
pdf. = 300 MPa	450.19	0.003	661.83	0.242
Welded joint AISI 316L				
tdf. = 6.5s	476.52	0.004	672.90	0.444
tdf. = 8.5s	482.43	0.004	658.07	0.468
tdf. = 10s	500.69	0.004	670.63	0.231

tdf. friction time, *pdf.* friction pressure

of this model on both welded and non-welded base metals showed a good fit for both base metals and mainly for AISI 316L. On the other hand, a poor fit was noted for the other three post-welded metals. The best fit was recorded for the AISI 316L combination, see Table 2. Practically, Ludwik's law gives better results for large deformations.

To write Eq. 2, only the second part of Ludwik's law and Hollomon's law Eq. 1 was used, neglecting the first term expressed by the stress σ_0. Plotting and linear regression of the latter rational stress-strain allowed us to determine the two other parameters (Fig. 5) called Hollomon parameters, which helped us to access the two strain-hardening parameters K_H and n_H, (shown in Table 3). From this plot, it can be seen that this second law shows the presence of a double hardening zone for the two base metals and for the post-welded metal AISI 316L. On the other hand, it shows only one zone for AISI 304L (Fig. 5).

In addition to the Swift power-law parameters, K_S and n_S, obtained by smoothing Eq. 4 and based on the Hollomon equation shown in Eq. 3, an additional term denoted by (ε_0) was included and considered a plastic pre-strain. The same remarks granted to Hollomon's law can be made regarding the presence of two strain hardening zones (Fig. 6). The difference between the latter two laws is that Swift's law is more accurate than Hollomon's law (Table 4).

To account for the small distortion deviations obtained using the first three previous laws, Ludwigson proposed to modify Hollomon's law by adding a second term that is represented by Eq. 7. The plot of this law, which is known as Ludwigson's law (Fig. 7) shows two linearly trending behaviors; the first one is in the large deformation domain (Eq. 8), and the second is in the small deformation domain (Eq. 9). In this law, the two parameters K_1 and n_1 are the parameters of Hollomon's law. On the other hand, it is defined by the difference between the experimental and Hollomon stress. Using Eq. 4, K_2 and n_2 can be obtained by linear regression of the equation: lnΔ - εp, and the obtained values are grouped in Table 5.

4 Discussion

4.1 Mechanical properties

Figure 2 shows the true tensile curves of the base metals called rational curves of similar and dissimilar welded joints. In addition, the mechanical properties of these metals are presented in Table 1. From these curves, it can be seen that

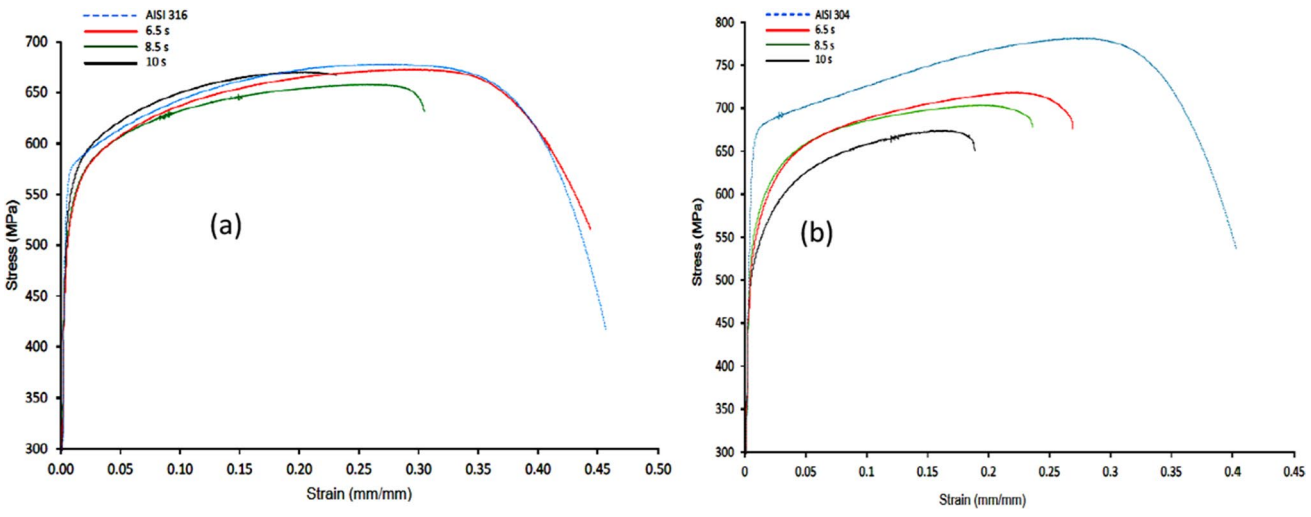

Fig. 3 **a** Tensile tests of the AISI 316L joint under three friction times and **b** tensile tests of AISI 304L gasket under three friction times and base metal

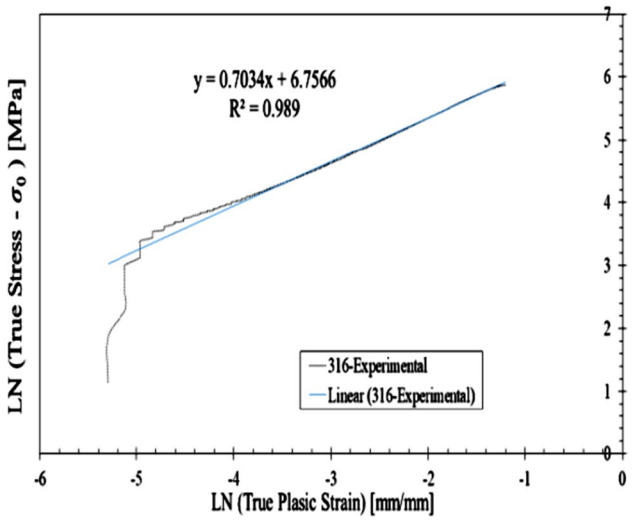

Fig. 4 An example for Ludwik's strain hardening curve

Table 2 Hardening parameters obtained by smoothing rational curves

Materials	z	*K*L (MPa)	n_L	R^2
Base material				
AISI 304L		920.57	0.6704	0.9665
AISI 316L		859.71	0.7034	0.9890
Welded joint				
AISI 304L	pdf. = 0 MPa	1020.14	0.5953	0.9203
	pdf. = 280 MPa	901.26	0.5498	
	pdf. = 300 MPa	999.74	0.5719	0.9268
AISI 316L	tdf. = 6.5s	851.67	0.5703	0.9591
	tdf. = 8.5s	788.31	0.5597	0.9527
	tdf. = 10s	807.46	0.5681	0.9468

tdf. friction time, *pdf.* friction pressure

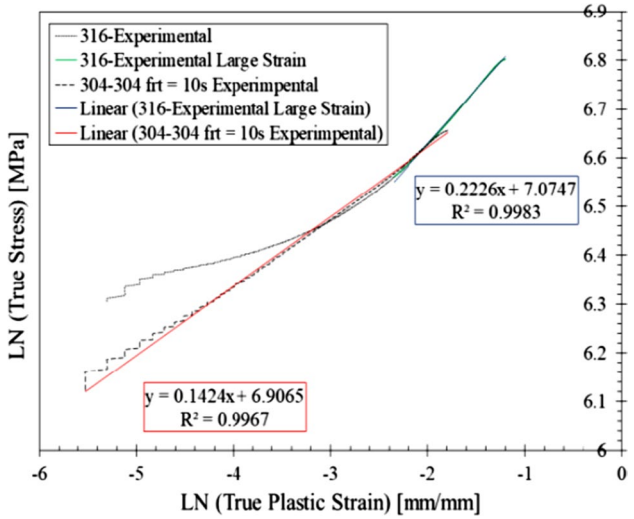

Fig. 5 An example for Hollomon's strain hardening curve

Table 3 Hardening parameters of Hollomon's law

Material		K_H (MPa)	n_H	*R*2
Base materials* (1)				
AISI 304L		1422.11	0.2539	0.9983
AISI 316L		1181.68	0.2226	0.9983
Welded joints				
AISI 304L	pdf. = 0 MPa	1096.41	0.1504	0.9873
	pdf. = 280 MPa	1043.56	0.1334	0.9906
	pdf. = 300 MPa	998.74	0.1424	0.9967
AISI 316L*	tdf. = 6.5s	1190.46	0.2330	0.9977
	tdf. = 8.5s	1117.22	0.2059	0.9969
	tdf. = 10s	1082.46	0.1759	0.9977

tdf. friction time, *strain hardening parameters for large deformations

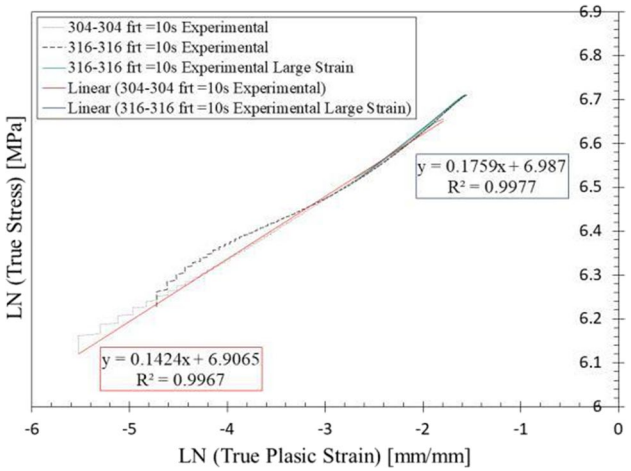

Fig. 6 Swift strain hardening curve

Table 4: Hardening parameters of Swift's law.

Materials		KS (MPa)	nS	ε0	R^2
Base metal* (in French)					
AISI 304L		1429.38	0.2612	0.0049	0.9985
AISI 316L		1182.04	0.2262	0.0049	0.9981
Welded joints	Time and pressure (*s*)				
AISI 304L	0 MPa	1123.72	0.165	0.0039	0.9928
	280 MPa	1070.09	0.1475	0.0039	0.9949
	300 MPa	1025.46	0.1558	0.0029	0.9992
AISI 316L*	6.5s	1194.28	0.2380	0.0039	0.9979
	8.5s	1121.69	0.2110	0.0039	0.9973
	10s	1089.09	0.1817	0.0039	0.9981

tdf. *strain hardening parameters at large strain

the yield strength of the similar and dissimilar welded joints has decreased compared to those of the base metals. In fact, for a friction time of 7 s, a decrease of about 19.25% can be

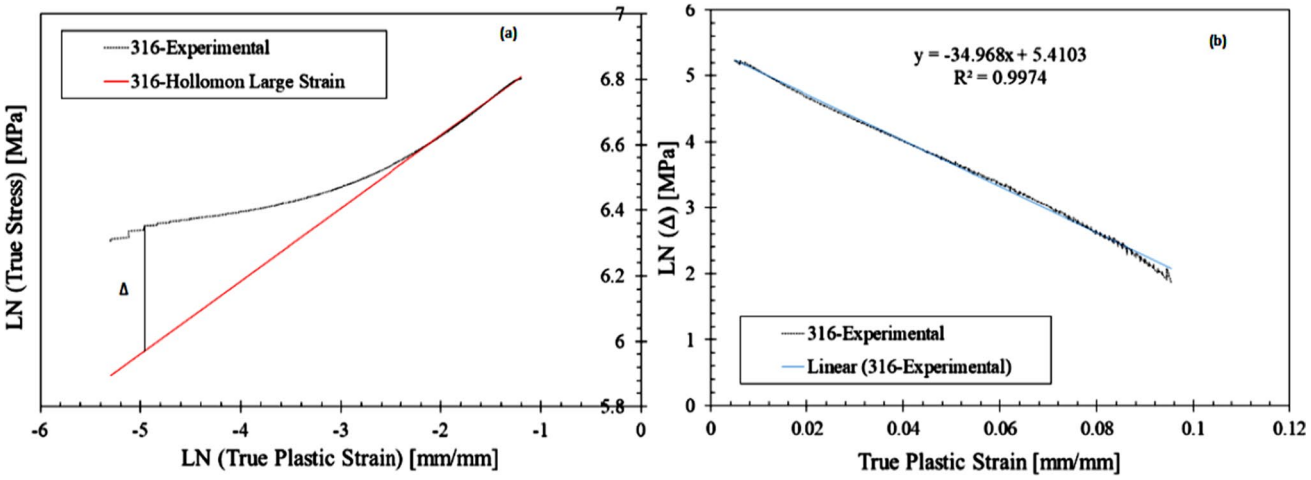

Fig. 7 Examples of a Ludwigson strain hardening curve

Table 5 Hardening parameters of Ludwigson's law

Metals		$K1$ (MPa)	n_1	K_2	n_2	R^2
Base metal						
AISI 304L		1422.11	0.2539	5.8759	−32.727	0.9890
AISI 316L		1181.68	0.2226	5.4103	−34.968	0.9974
Welded joints						
AISI 316L	tdf. = 6.5s	1190.46	0.233	5.2414	−28.323	0.9953
	tdf. = 8.5s	1117.22	0.2059	5.1095	−31.83	0.9905
	tdf. = 10s	1082.46	0.1759	4.9194	−44.216	0.9923

observed for the AISI 304L joint and 12% for the AISI 316L joint. These results confirm a high stiffness of the AISI 304L metal compared to the AISI 316L substrate. On the other hand, there is a higher ductility for the AISI 316L, which is contrary to the AISI 304L metal. As an example, for a friction time of 7 s, a decrease in ductility of the order of 2.84% can be noted for the joint AISI 316 and 30.12% for the joint AISI 304L, respectively. Moreover, it was observed that for a similar welded joint with a longer friction time, low tensile strength, low ductility, a high level of micro-hardness, and high plastically deformed zone (HPDZ), while for a shorter friction time, an opposite trend was obtained as a result of the accumulated heat at the joint not having enough time to diffuse. More details on the microhardness and the HPDZ influence on the AISI 204L and AISI 316L are available elsewhere [1, 20].

Therefore, the use of higher rotational speed and shorter friction time can increase the maximum stress of the welded joint [7]. On the other hand, for a dissimilar joint, high ductility was recorded with a friction time of 6.5 s and high tensile strength in the case of a friction time of 8.5 s. This can be attributed to the mechanical and thermophysical properties of the post-weld strain hardening of the dissimilar joint that mainly influence the mechanical behavior of this type of joint, as the temperature reached by each joint is dependent on the thermophysical properties of the two metals to be welded and the selected friction time [1]. Therefore, the stress-temperature relationships for each joint should affect the joint properties resulting from the welding operation [20]. A short friction time of 6.5 s has shown a hardening at the rotating part and softening at the fixed part, which signified the weak mechanical action related to the rotating part. However, at a longer friction time of 10 s, a symmetrical shape of the softening profile on both sides was observed. In the same process, for the seal AISI 304L, we can see a general softening of the fracture face. At a shorter friction time of 6.5 s, the highly plastically deformed zone (HPDZ) was found on the AISI 316L joint. Therefore, at a longer friction time of 8.5 s, the HPDZ has an average value for the AISI 304L [1].

4.2 Hardening capacity

The hardenability of a material can be considered a ratio of the ultimate tensile strength σ_{max} to the yield strength σ_Y [22, 23]. Chiu et al. [22] redefined a normalized hardenability parameter denoted by H_c, as follows:

$$H_C = \frac{\sigma_{max} - \sigma_Y}{\sigma_Y} = \frac{\sigma_{max}}{\sigma_Y} - 1 \quad (10)$$

The curing ability of base metals and similar and dissimilar welded joints is shown in Table 6. We found an improvement in the curing ability of the welded joints compared to the base metals. In the case of similar welded joints, there was a higher curing ability of the AISI 304-AISI 304 joint due to a higher curing ability of the AISI 304 base metal. Similarly, a higher curing capacity was obtained on dissimilar AISI 304L welded joints, and the curing capacity decreased with friction time for the AISI 316 joint but increased for the AISI 304L joint. The hardening capacity of a material is normally related to its yield strength which can be furthermore associated with the microstructure and texture of the material.

An increase in the grain size should decrease the value of the yield strength according to the Hall-Petch relationship and increase the storage capacity of dislocations, leading to a higher hardening capacity [24–26]. A decrease in grain size reduces the difference in flow resistance between the grain boundary and the interior, which in turn reduces the hardening capacity [27–30]. However, the hardening capacity of similar welded joints is higher than that of base metals despite the grain refinement observed in the HPDZ (Fig. 3).

Table 6 Strain hardening capacity of the base material and the welded joint

Metals	σy (MPa)	σmax (MPa)	HC
AISI 304L	618.74	781.41	0.27
AISI 316L	541.47	678.19	0.25
AISI 304 tdf. = 0 s	499.59	718.11	0.43
AISI 304L tdf. = 5 s	502.91	703.68	0.39
AISI 304L tdf. = 8 s	450.19	661.83	0.47
AISI 316L tdf. = 4s	476.52	672.90	0.41
AISI 316L tdf. = 5 s	482.43	658.07	0.36
AISI 316L tdf. = 6.5 s	500.69	670.63	0.33
AISI 316L tdf. = 8.5 s	427.94	629.40	0.47
AISI 304L tdf. = 10 s	453.48	677.12	0.49

4.3 Modeling of post-weld hardening

In this part of our work, we were interested in modeling the isotropic strain hardening behavior using four laws identified in the previous discussion, in which we worked on two base metals (Fig. 8a and b) before treating the welded joints. From these figures, we noticed a good similarity between the Ludwik and Ludwigson laws of behavior with better accuracy for the second model in predicting the behavior of AISI 304L and AISI 316L. Figure 8a shows a small deviation in the low deformation region of the experimental curve.

Secondly, from the post-weld results, we can state that both Ludwik's and Ludwigson's laws give better predictions for AISI 316L with a friction time of 8.5 s (Fig. 9). On the other hand, the Hollomon and Swift models, provided the same results for the two remaining times, 6.5 s and 10 s for the AISI 316L substrate (Figs. 9 and 10). Based on the above, we can reveal that Ludwigson's law has a better description of the behavior of the two separate base metals and of the AISI 316L combination. On the other hand, fitting the experimental data showed better quality to Swift's model than Hollomon's model for both combinations for the AISI 304L.

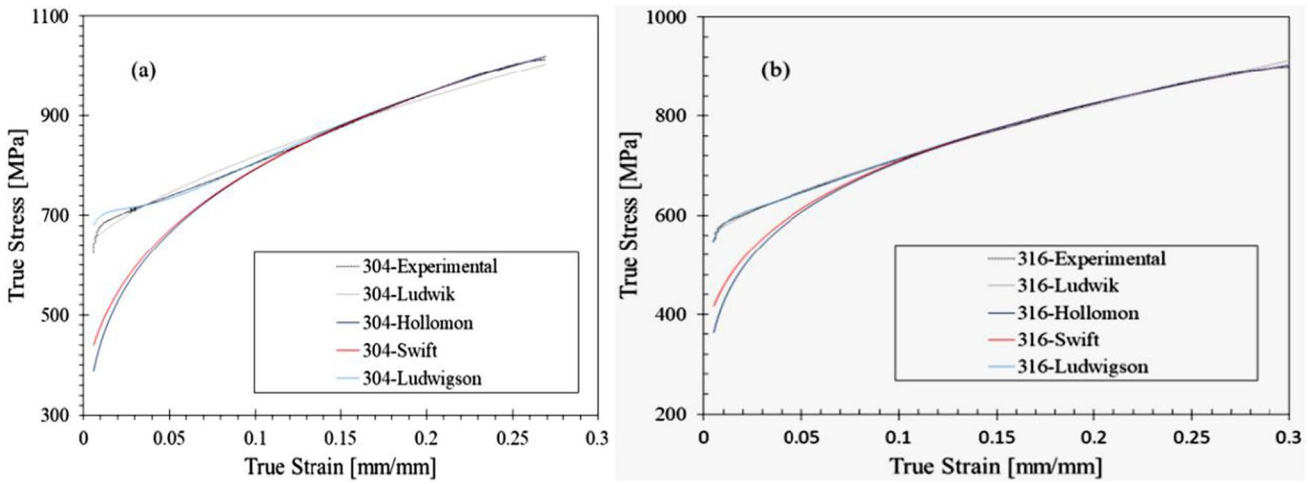

Fig. 8 Comparison of the tested models against the obtained experimental results for the two base materials

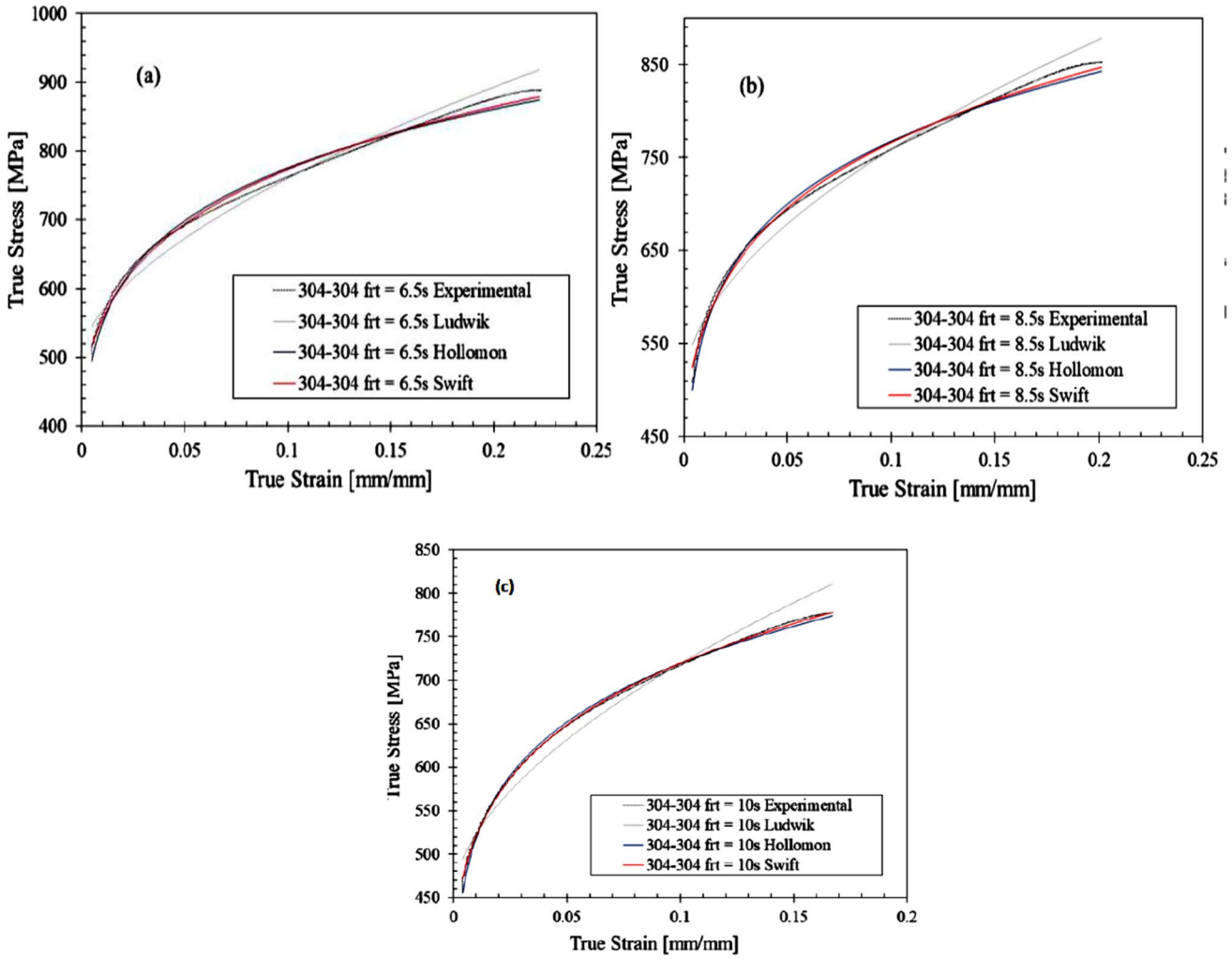

Fig. 9 Effect of friction pressure on post-weld work hardening, AISI 304L

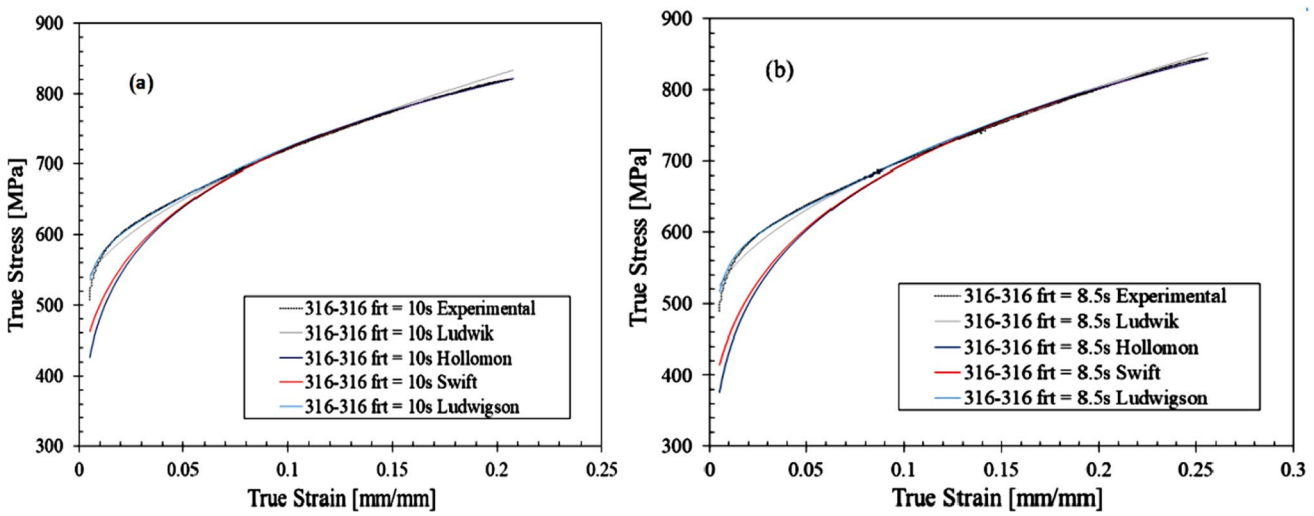

Fig. 10 Effect of friction time on the post-weld hardening of AISI 316L for **a** 10 s and **b** 8.5 s

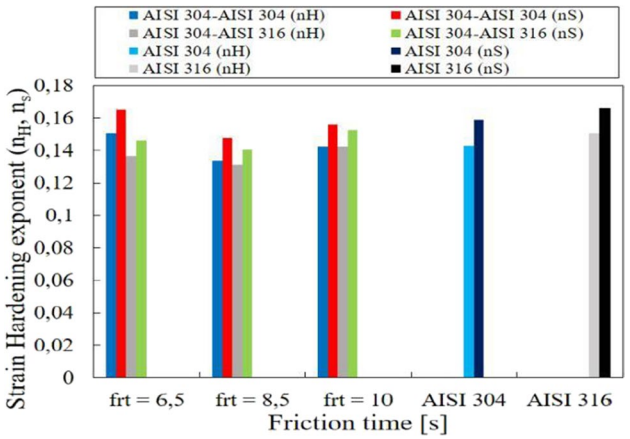

Fig. 11 Evolution of the strain hardening exponent as a function of the friction time, AISI 304L and AISI 316L

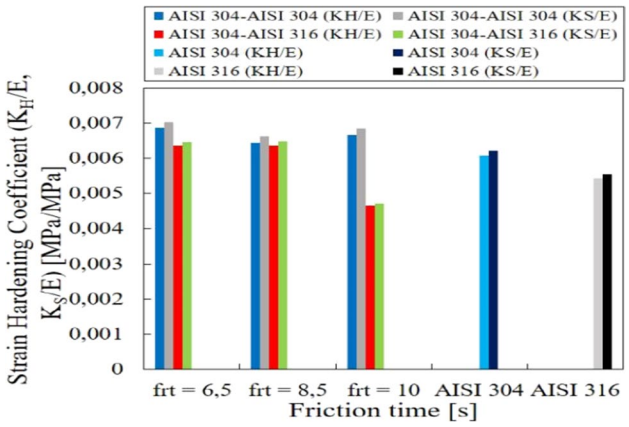

Fig. 12 Evolution of the normalized strain hardening coefficient (K/E) as a function of the friction time, AISI 304L

4.4 Evolution of curing parameters as a function of friction time

The strain hardening exponent was evaluated by Hollomon's and Swift's laws for both AISI 304L and AISI 316L joints, and the results are depicted in Fig. 11, whereas the strain hardening exponent was evaluated by the Ludwigson's law for the AISI 316L joint (Fig. 11). The strain hardening exponent is a measure of a metal's ability to work-harden; the larger its magnitude, the greater the strain hardening for a given amount of plastic deformation [24, 31]. The higher the value (n), the more the material can deform before instability and can be stretched further before the onset of straining [27, 32–37]. From Fig. 11, it can be seen that the hardening exponent of the AISI 304L joint, for a friction time of 6.5 s, is higher than that of the AISI 304L base metal, which corresponds to a higher hardening. The strain hardening exponent was reduced at a friction time of 8.5 s and then increased again at a friction time of 10 s. Note that the strain hardening exponent took the maximum value for a friction time of 10 s corresponding to the highest hardening.

The variations of the normalized strain hardening coefficient (K/E) as a function of friction time for the two combinations AISI 304L and AISI 316L using both Hollomon's and Swift's laws are shown in Fig. 12. It can be seen that the normalized strain hardening coefficient has a maximum value for the AISI 304L-AISI 304L joint at a friction time of 6.5 s, then decreased for the 8.5 s time, and rose again at a friction time of 10 s. In the case of the AISI 304L joint, it can be seen that the values of the normalized strain hardening coefficient were very close for friction times 6.5 s and 8.5s. The maximum values were recorded for the welded joint at 8.5 s and a remarkable decrease was observed for a friction time of 10 s. From Fig. 13a, it is observed that the strain hardening exponent n_1 decreased as the friction time increased for the AISI 316L joint. Similar behavior was noted for the two other parameters of Ludwigson's law n_2 and K_2 (Fig. 13b). Compared to the parent metal, the strain hardening exponent n_1 reached its maximum value for a friction time of 6.5 s corresponding to the highest strain hardening.

4.5 Analysis of fracture surfaces

The fracture surfaces observed by the SEM technique of similar joints are shown in Fig. 14. Dimples are observed in the fracture surface of all welded joints indicating that the primary failure mechanism is ductile; the same observations are noted by [28, 38–41]. These fracture surfaces exhibited a combination of equiaxed dimples and elongated dimples at all welded joints, which indicated a shear movement of the material in this region. A ductile fracture in all welded joints was observed to occur in three stages: (1) void nucleation, (2) void growth, and (3) void coalescence resulting in a dimpled fracture surface.

Crack extension in the welding joint of the two grades of steel is governed by ductile failure mechanism, namely, the nucleation of microvoids and the growth and coalescence of these microvoids. However, for the dissimilar AISI 304L/AISI 306L joint at different friction times, voids close to the void are not elongated along the direction of loading but along the shearing stress direction component that induced failure by mode II superimposed with mode I. Therefore, the crack extension has a zigzag path characteristic of mixed mode (I + II) failure mode. This zigzag mechanism can be seen in Fig. 14a and b. The crack path is linear along a direction that is close to the pure mode II bifurcation angle (see Fig. 14a,b). Therefore, ductile crack extension is governed by the intensity of the shearing mode induced by the difference in dissimilar inclusions. Due to hard particles inside voids (these particles promote void nucleation by stress

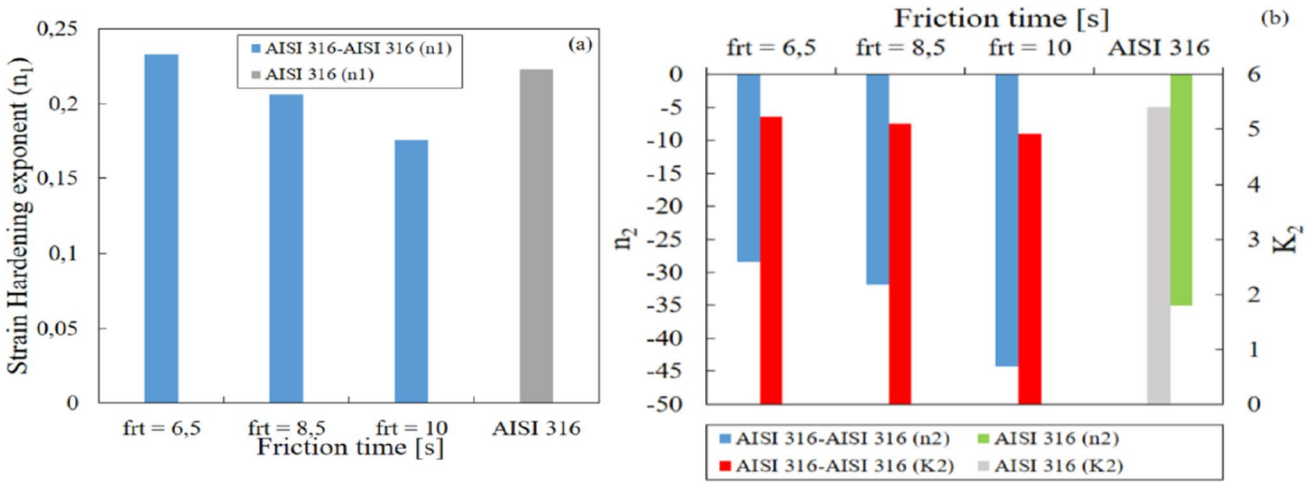

Fig. 13 Evolution of the hardening parameters as a function of the friction time, AISI 316L

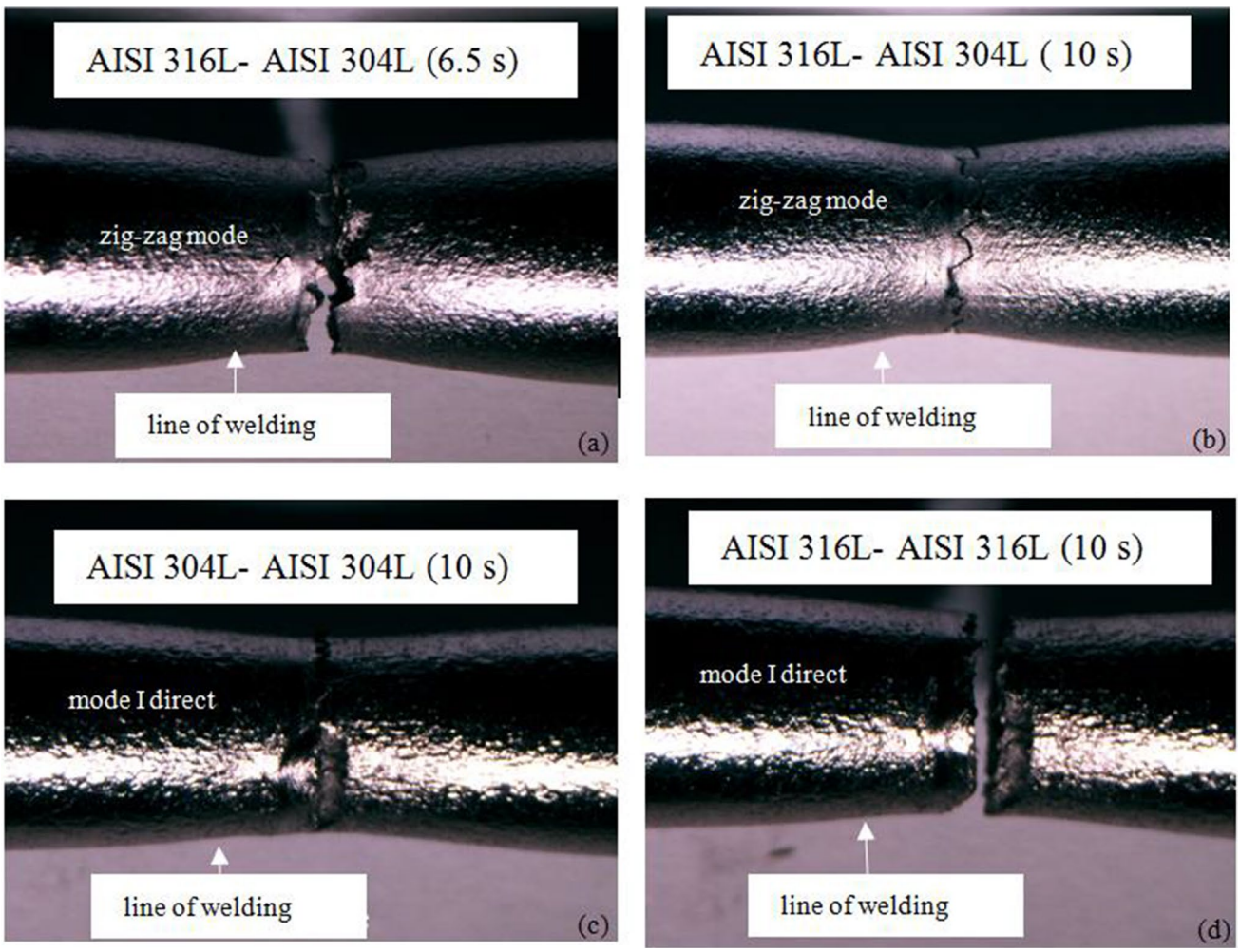

Fig. 14 Position of the tensile fracture with a similar grade

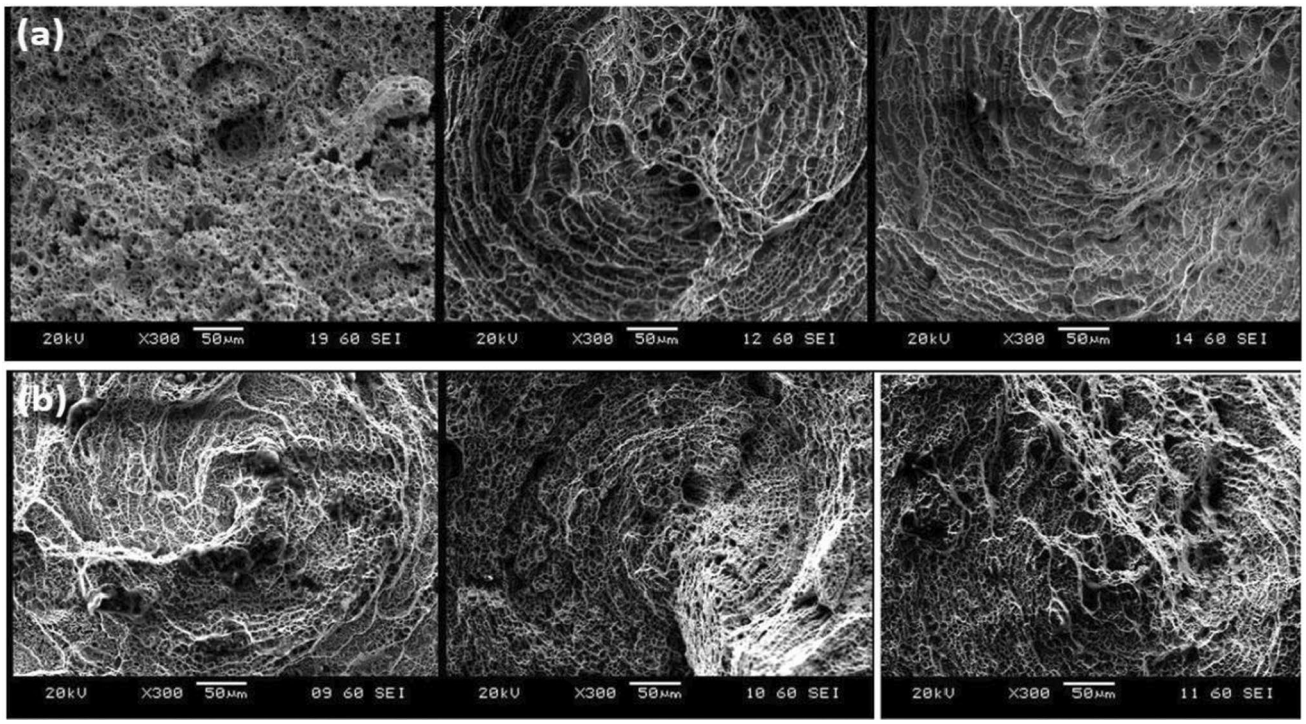

Fig. 15 SEM observation, **a** AISI316, **b** AISI 304L, for three friction times (6.5, 8.5 and 10 s)

concentration), voids cannot be closed by compressive stress, and crack extension is then stable in the void direction according to the scheme in Fig. 14c and d for the similar grade. If the stress is positive and higher than the opening stress at some distance ahead of the void tip, dislocation extension then occurs in the principal direction, which corresponds to the maximum stress direction.

Some wide and deep dimples in the AISI 316L welded joint at a friction time of 6.5 s and 8.5 s suggested a high elongation before failure, while thin and shallow dimples in the case of an AISI 316L welded joint at a friction time of 10 s indicated limited elongation and high strength before failure (Fig. 15a). In addition, it was observed that the AISI 304L joint (Fig. 15b) has a greater capacity for thermoplastic deformation than both AISI 316L and AISI 304L joints demonstrated by the absence of a spiral shape on the fracture surface and resulting from the metal flow that occurs near the plane of the weld causing the rotating part to move against the fixed part [41–52].

5 Conclusion

This study analyzed the work-hardening behavior of two austenitic steels AISI 304L and AISI 316L that were welded separately by direct friction. The use of behavior laws allowed us to elucidate the role of strain hardening generated by post-welding friction. The laws of Hollomon and Swift showed the presence of a double zone of hardening for the two joints AISI 304L and AISI 316L. On the other hand, it showed only one zone for the AISI 304L metal. Based on our obtained experimental results in this study, the two analytical laws of Ludwik and Ludwigson, in our opinion, can be used safely to describe the strain hardening behavior for the two base metals AISI 304L and AISI 316L. However, Swift's law gave better results and greater accuracy than the other laws in describing the strain hardening behavior of the AISI 304L and AISI 316L materials. Finally, we found that Ludwigson's law is the most suitable model to describe the behavior of AISI 316L metal. The highest strain hardening exponent was recorded for (i) AISI 304L at a pressure of 280 and 300 MPa and (ii) for the AISI 316L metal at a friction time of 6.5, 8.5, and 10 s.

On the other hand, we noted that the best post-welding mechanical properties were obtained for the time of 8.5 s, while the highest work-hardening exponent was recorded at a friction time of 6.5 s for the AISI 316L joint. The welding of the basic materials AISI 316L and AISI 304L allowed us to obtain joints with better mechanical properties for a friction time of 6.5 s. On the other hand, the AISI 304L joint, for a friction time of 8.5 s, gave better mechanical properties.

Author contributions FZ.A, A.M., and M.H.M. conceived and designed the experiments; FZ.A. carried out the experiments; M.H.M and R.K.S. analyzed the experimental data and wrote the manuscript. All authors have read and agreed to the published version of the manuscript.

Declarations

Conflict of interest The authors declare no competing interests.

References

1. Hassan AJ, Boukharouba T, Miroud D, Ramtani S (2019) Metallurgical and mechanical behavior of AISI 316- AISI 304 during friction welding process. Int J Eng Transactions B: Applications 32(2):284–291. https://doi.org/10.5829/ije.2019.32.02b.16
2. Vill VI (1962) Friction welding of metals. American Welding Society, Inc, New York
3. Kimura M, Kusaka M, Kaizu K, Nakata K, Nagatsuka K (2016) Friction welding technique and joint properties of thin-walled pipe friction welded joint between type 6063 aluminum alloy and AISI 304 austenitic stainless steel. Int J Adv Manuf Technol 82:489–499
4. T.J., Jessop and W.O., Dinsdale, Friction welding dissimilar metals, Proc. of Master-Maintenance industrielle et fiabilité-Université Badji Mokhtar Annaba-Annaba-Algérie.
5. Samene, A. et Harem, M., Optimisation des paramètres de procède du soudage par friction rotative, 2017. Mémoire de Master – Génie mécanique, Université Mohamed El-Bachir El Ibrahimi-Bordj Bou Arreridj-Algérie.
6. Hamza S, Boumerzoug Z, Raouache E, Delaunois F (2019) Simulated heat affected zone in welded stainless steel 304L. Acta Metall Slovaca 25(3):251–258
7. Kweon H, Kim J, Song O, Oh D (2020) Determination of true stress-strain curve of type 304 and 316 stainless steels using a typical tensile test and finite element analysis. Nucl Eng Technol 53. https://doi.org/10.1016/j.net.2020.07.014
8. Niyazi Ozdemir, Firat University, Sarsılmaz F, Hasçalık A Effect of rotational speed on the interface properties of friction-welded AISI 304L to 4340 steel. Mater Des (1980-2015) 28(1):301–307
9. Attallah MM, Preuss M (2012) Inertia friction welding (IFW) for aerospace applications. Welding Joining of Aerospace Mater:25–74
10. Nasution AK, Murni NS, Sing NB, Idris MH, Hermawan H (2015) Partially degradable friction-welded pure iron–stainless steel 316L bone pin. J Biomed Mater Res Part B Appl Biomater 103:31–38
11. Ludwik P (1909) Elemente der Technologischen Mechanic, Verl. Julius Springer 32
12. Hollomon JH (1945) Tensile deformation. Trans AIME 162:268–290
13. Swift HW (1952) Plastic instability under plane stress. J Mech Phys Solids 1:1–18
14. Ludwigson DC (1971) Modified stress-strain relation for FCC metals and alloys. Metall Trans A 2:2825–2828
15. Kumar JMB, Bahaa Saleh H, Fayaz AC, Gera T, Nisar KS, Saleel CA (2023) Experimental and analytical investigation on friction welding dissimilar joints for aerospace applications. Ain Shams Eng J 14(2):101853
16. Pratyusha M, Ramana PV, Prasanthi G (2021) Evaluation of tensile strength of dissimilar metal pure aluminium and pure copper friction welds. Mater Today Proc 38:2271–2274
17. Delgado-Pamanes M, Alvarez-Montufar J, Reyes-Osorio L, Garza C, Suárez-Rosales M, Chávez-Alcalá J (2022) Evaluation of optimal processing parameters for a Zn-based eutectoid alloy processed by friction-stir welding. J Mater Res Technol 18:3256–3265
18. Li F, Liu Y, Ke W, Jin P, Kong H, Chen M, Sun Q (2022) A novel pathway to weld forming control and microstructure improvement of duplex stainless steel via alternating magnetic field. J Manuf Process 80:581–590
19. Li L, Du Z, Sheng X, Zhao M, Song L, Han B, Li X (2022) Comparative analysis of GTAW+SMAW and GTAW welded joints of duplex stainless steel 2205 pipe. Int J Press Vessel Pip 199:104748
20. Arzour FZ, Hadj Meliani M, Jabbar A, Boukharouba T (2020) Microstructure evolution in friction welding of AISI 316. Structural Integrety and Life 20(01)
21. Samuel KG (2006) Limitations of Hollomon and Ludwigson stress-strain relations in assessing the strain hardening parameters. J Phys D Appl Phys 39:203–212
22. Ramirez AJ, Benati DM, Fals HC (2011) Effect of tool offset on dissimilar Cu-AISI 316 stainless steel friction stir welding. In: Proceeding of the 21st International Offshore and Polar Engineering Conference, vol 8, USA, pp 548–551
23. Chiu KY, Cheng FT, Man HC (2005) Laser cladding of austenitic stainless steel using NiTi strips for resisting cavitation erosion. Mater Sci Eng A 402(1-2):126–134
24. Murry G, Aciers. Généralités. (1993) Techniques de l'ingénieur. Génie mécanique (M300):1–29
25. Ben Kechroud Basma, (2014). Comparative study of four steels for pipeline for Sonatrach made at TSS Arcelormittal-Annaba according to physico chemical parameters and choice of steel X52. Master thesis- Mechanics of materials- University Badji Mokhtar Annaba-Annaba-Algeria.
26. Hannouf B, Zeddam A (2018) Use of soft computing techniques in a non-destructive testing process" Master's thesis,. University of Jijel
27. Putz A, Hosseini VA, Westin EM, Enzinger N (2020) Microstructure investigation of duplex stainless steel welds using arc heat treatment technique. Weld World 64:1135–1147
28. Cao F, Huang G, Hou W, Ni R, Sun T, Hu J, Shen Y, Gerlich AP (2022) Simultaneously enhanced strength-ductility synergy and corrosion resistance in submerged friction stir welded super duplex stainless steel joint via creating ultrafine microstructure. J Mater Process Technol 307:117660
29. Nathalie KOPP (1999) Contribution to the characterization of butt weld defects in low alloy steel by ultrasonic non-destructive testing. University of Metz, France
30. French standard A 09-325 Non-destructive testing ultrasonic beam -Generalities-September-198.
31. Kada Karim and gharabi tayab (2018) Non-destructive testing; electrical networks; Ahmed doraya University. Adrar Faculty of Science and Technology Department of Electrical Engineering
32. Adnene Tlilli; Sofien Marzouki; Non-destructive testing; Institut supérieur des études technologiques de Jendouba. Industrial Maintenance Department; 2005/2006; Tunisia.
33. Raid A (2017-2018) Non-destructive testing; penetrant testing, magnetoscopy, radiography, eddy current and ultrasonics. University of Science and Technology of Oran Mohamed-Boudiaf
34. Sloderbach Z, Pajak J (2005) Determination of ranges of components of heat affected zone including changes of structure. Arch Metall Mater 60(4):2607–2612
35. Beranger G, Henry G, Sanz G (1994) ≪Le livre de l'acier≫. Technique et Documentation, Lavoisier
36. Helal Y (2017) thesis "The effect of friction stir welding on the microstructure and mechanical properties of a welded joint composed of an industrial aluminum alloy and a steel". Mohammed Khaider University Biskra

37. Gerard M (2010) thesis "Heterogeneous diffusion welding assisted by friction stirring, case of the Al/Fe couple". Ecole Centrale de Nantes
38. Review by Dr. Ir. Koen Faes, IBS (Translation: M.C. Ritzen), Belgian Welding Institute.
39. REVIEW friction welding - critical assessment of literature. Maalekian, M. Graz University of Technology: sn, 09 10 2007, Institute of Materials, Minerals and Mining, pp 738-759.
40. Jeffus L (2012) Welding: principles and applications, 7th edn. DELMAR Cengage Learning, USA
41. Maeder T, N'Guyen Q, Weber L (2006. LMM Laboratory - Quoted on pages 35) "Techniques d'assemblage - le soudage en phase solide", course, Ecole Polytechnique Federale de Lausanne (EPFL). Lausane 36:39
42. Cazès R (1996) Soudage par friction. Techniques de l'Ingénieur B7745:37
43. Pichot F, Corpace F (2014) Aerospace engine design and manufacturing. SAFRAN Group (SNECMA)
44. Jamaludin SB, Keat YC, Ahmad ZA (2004) The effect of varying process parameters on the microhardness and microstructure of Cu-steel and Al-Al2O3 friction joints. J Teknol 41:85–95
45. Li W, Vairis A, Preuss M, Tiejun MA (2016) Linear and rotary friction welding review. Int Mater Rev
46. Sathiya P, Aravindan S, Haq AN (2007) Effect of friction welding parameters on mechanical and metallurgical properties of ferritic stainless steel. Int J Adv Manuf Technol 31(11):1076–1082
47. Uday MB, Ahmad Fauzi MN, Zuhailawati H, Ismail AB (2010) Advances in friction welding process: a review. Sci Technol Weld Join 15(7):534–558
48. D.D. Kautz, "Fundamentals of friction welding," ASM Handbook, Volume 6A, Welding Fundamentals and Processes, 2011.
49. Koen Faes, (IBS): friction welding (translation: M.C. Ritzen-IBS. BIL), http://www.bil-ibs.be/fr/soudage-par-friction. (Apr. 12, 2018).
50. Ananda Rao G, Ramanaiah N (2019) Dissimilar metals AISI 304 steel and AA 2219 aluminium alloy joining by friction welding method. Mater Today Proc 19:902–907
51. Li W, Suo J, Ma T, Feng Y, Kim K (2014) Abnormal microstructure in the weld zone of linear friction welded Ti–6.5Al–3.5Mo–1.5Zr–0.3Si titanium alloy joint and its influence on joint properties. Mater Sci Eng A 599:38–45
52. Tasalloti H, Kah P, Martikainen J (2017) Effect of heat input on dissimilar welds of ultra high strength steel and duplex stainless steel: microstructural and compositional analysis. Mater Charact 123:29–41